Effect of Cenosphere Filler Surface Treatment on the Erosion Behavior of Epoxy Matrix Syntactic Foams

Kiran Shahapurkar,[1] Mrityunjay Doddamani,[1] G.C. Mohan Kumar,[1] Nikhil Gupta[2]
[1]*Lightweight Materials Laboratory, Department of Mechanical Engineering, National Institute of Technology Karnataka, Surathkal, 575025, India*

[2]*Composite Materials and Mechanics Laboratory, Mechanical and Aerospace Engineering Department, Tandon School of Engineering, New York University, Brooklyn, New York, 11201, USA*

Influence of cenosphere surface modification and volume fraction on the solid particle erosion of cenosphere/epoxy syntactic foams is investigated. Fly ash cenospheres are used as filler in both as received and silane surface modified configurations. Erosion behavior is studied at room temperature for different impact angles (30, 45, 60, and 90°) and velocities (30, 45, and 60 m/s). Neat epoxy shows the highest erosion rate compared with that of the syntactic foams. Results show a strong dependence of impact angle and velocity on erosion rate of syntactic foams. With increasing cenosphere content erosion rate decreases for all impact angles. Erosion rate decreases with increasing impact angle and with decreasing velocity. Good interfacial bonding of treated cenospheres enhances the erosion resistance. All the samples exhibit ductile erosive behavior, with maximum erosion at 30°. The velocity exponent and erosion efficiency parameters confirm the ductile behavior of syntactic foams. POLYM. COMPOS., 40:2109–2118, 2019. © 2018 Society of Plastics Engineers

INTRODUCTION

Weight sensitive structures require materials with high specific properties, which have led to development of lightweight syntactic foam composites. Syntactic foams are composites formed by dispersing hollow particles in the matrix resin. Automobile, aerospace and marine applications extensively use such foams due to their excellent specific properties [1–3]. Generally, reinforcements in polymers are used for a variety of reasons such as reducing the use of expensive resin, density control and tailoring optical, thermal, mechanical and electrical properties. The inclusion of such particulate fillers into polymers is primarily targeted at cost saving and improvement in specific properties [4–6]. Synergistic effects of higher modulus and reduced material cost are observed by incorporating hard filler particles into polymers [7]. Fly ash is one such filler, which is a waste by-product derived from thermal power plants [8,9]. It contains hollow particles called cenospheres [10,11] which comprises alumina, silica and iron oxides as the main constituents. Fly ash disposal is a challenge and finding beneficial usage of this industrial waste material in synthesizing syntactic foams can provide high performance composites at low cost [9,12–14]. Fly ash cenospheres are used to develop hybrid syntactic foams of metal with clay with focus on wear resistant applications [15]. Presence of cenospheres in cement paste lowers moisture absorption making them most suitable in construction sector [16]. In structural applications in vehicles, these foams can come across a verity of loading conditions, including erosion, which is the focus of this work.

Progressive removal of material from a target surface owing to the repeated impact of solid particles is termed as erosion [17]. Erosion depends on a number of factors like the physical and chemical properties of the erodent, surface morphology of constituents material system under investigation, filler content and the experimental conditions used [18]. Interaction of erodent with the specimen and the rebounding effects at the interface occur simultaneously during erosion. The resistance to erosion for various types of polymers and their composites has been studied by a number of researchers [19,20]. It is reported that the solid particle erosion is governed by the impingement angle, particle size, shape and hardness [21].

Although, extensive reports are available on the erosive behavior of composites [17,22–24], studies on syntactic foams are scarce. This work is carried out to investigate the erosion behavior of cenospheres reinforced syntactic foams. The study parameters include filler content, impingement angle and impact velocity. Further, results of as received and silane-treated cenosphere filled epoxy foams are compared with determine the effects of particle surface coating

Correspondence to: M. Doddamani; e-mail: mrdoddamani@nitk.edu.in
Contract grant sponsor: Office of Naval Research; contract grant number: N00014-10-1-0988. contract grant sponsor: Department of Science and Technology; contract grant number: DST/TSG/AMT/2015/394/G.
DOI 10.1002/pc.24994
Published online in Wiley Online Library (wileyonlinelibrary.com).

on erosion behavior of the composite. Profilometry and scanning electron microscopy are carried out to study the extent and the mechanism of erosion.

MATERIALS AND METHODS

Materials

Lapox L-12 epoxy resin with K-6 hardener, supplied by Atul, Valsad, Gujarat, India, is used as the matrix. Fly ash cenospheres of CIL 150 grade procured from Cenosphere India Ltd., Kolkata, India are used as filler. The cenospheres have densities of 920 and 1,000 kg/m^3 in the as received and silane-treated conditions. Syntactic foams are prepared with as received and surface modified cenospheres. Silane coating on cenospheres is carried out using 3-Amino propyl triethoxy silane, obtained from Sigma Aldrich, Bangalore, India. Surface treatment of cenospheres is performed according to the procedure outlined in an earlier publication [25]. The silane coating on the cenospheres is confirmed by Fourier transform infrared spectroscopy. X-ray diffraction and particle size analysis of as received and silane-modified cenospheres are carried out and are reported previously in [26]. SiC particles are used as erodent. Particle size analysis on SiC erodent is also carried out with the procedure outlined in Ref. 26.

Sample Preparation

Syntactic foams are fabricated by mixing measured quantity of Lapox L-12 epoxy resin and cenospheres until a uniform slurry is obtained. Subsequently, hardener is added to the mixture prior to pouring into the aluminum mold having dimensions of 55 × 65 × 4 mm^3. The cast slabs are cured at room temperature for 24 h and post-cured at 90°C for 3 h. The mold cavity is coated with a silicone releasing agent. Syntactic foams with 20, 40, and 60 vol% cenospheres (as received and silane treated) are fabricated. The cast slabs are trimmed according to ASTM G76 standard. Neat epoxy slabs are also prepared under similar processing conditions for comparison. Samples are named according to the convention EXX-Y where E denotes epoxy resin, XX denotes vol% of cenospheres and Y represents filler modification condition (U-untreated and T-treated).

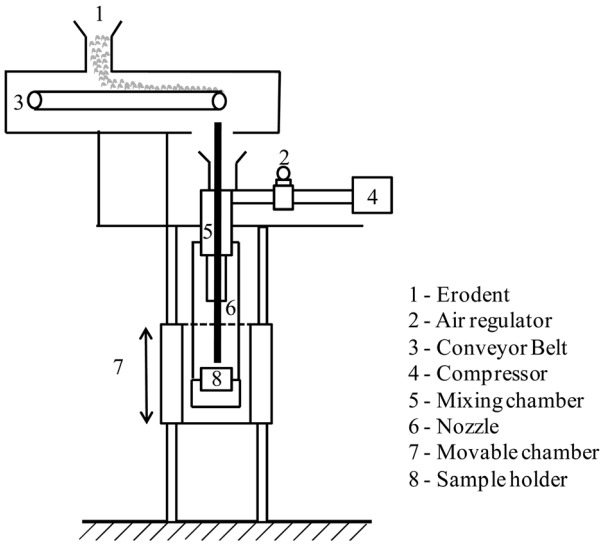

FIG. 1. Schematic of erosion test setup [35].

Hardness (H) is determined using Shore D hardness tester (IKON, IK/HTSD/01, India) with a hardened steel rod indenter of 1.4-mm diameter having 30° conical point and 0.1-mm radius tip.

The theoretical density of syntactic foams (ρth) is computed using rule of mixture.

$$\rho^{\text{th}} = \rho_{\text{f}} V_{\text{f}} + \rho_{\text{m}} V_{\text{m}} \tag{1}$$

where subscripts f and m denote filler and matrix, respectively and V denotes volume fraction. The densities of syntactic foams are experimentally measured according to ASTM D792–13.The entrapped matrix void volume content (φ_{V}) is estimated using theoretical and experimental (ρ^{exp}) densities of syntactic foams by,

$$\varphi_{\text{V}} = \frac{\left(\rho^{\text{th}} - \rho^{\text{exp}}\right)}{\rho^{\text{th}}} \tag{2}$$

The matrix void content significantly affects the properties and needs to be minimized.

Solid Particle Erosion Test

Erosion tests are performed under conditions as outlined in ASTM G76–13 standard [27] using a test rig (Fig. 1) procured from DUCOM, Bangalore, India. Compressed dry air is used to accelerate 5 g of erodent particles per minute to strike the test sample. Erosion test parameter values are listed in Table 1 and are chosen based on the literature [28,29]. Specimen surface is cleaned with acetone to remove the impurities. Subsequently all the specimens are

TABLE 1. Erosion test parameters [26,27]

Erosion parameters	Parameter	Value
Constants	Erodent	Silicon carbide
	Erodent size (μm)	250
	Erodent shape	Angular
	Test temperature (°C)	Room temperature
	Erodent mass flow rate (g/min)	5
	Nozzle to sample distance [10]	10
	Nozzle diameter [10]	1.5
	Nozzle length [10]	86
Variables	Impingement angle (°)	30, 45, 60, 90
	Impact velocity (m/s)	30, 45, 60
	Cenosphere content (vol%)	0, 20, 40, 60

DOI 10.1002/pc

weighed to an accuracy of 0.001 mg using a precision electronic balance (BSA223S, SARTORIUS, Germany). The specimens are firmly fixed in the sample holder and then the tests are carried out for 5 min at a predetermined erodent velocity and then the specimen weight loss is recorded. The test is continued and the weight is recorded every 2 min until the steady state of weight loss is achieved [27]. Total time of test is recorded to estimate erosion rate (ratio of sample weight loss to weight of eroding particles) [30]. At least five specimens are tested for each test condition and the average values are reported.

Imaging and 3D Profilometery

Scanning electron microscope (JSM 6380LA, JEOL, Japan) is used for micrographic analysis of as cast and eroded specimens. All the specimens are sputter coated with gold prior to imaging (JEOL JFC-1600, Japan). Nikon D 7000 camera with Nikkor 35 mm F1.8G lens is used for imaging the erosion profile. 3D profiles of the eroded samples are obtained using optical profilometry (ZETA-20, ZETA Instruments, USA).

RESULTS AND DISCUSSIONS

Particle Size Analysis of Erodent

The shape of the erodent SiC particles is irregular (Fig. 2a). The angularity in the SiC particles may assist in fracturing the thin walled hollow cenospheres, particularly at lower impact angles. Figure 2b shows size analysis of SiC particles. Weighted mean particle size is observed to be 249.1 μm.

Material Microstructure

Micrographs of as cast syntactic foams show uniform dispersion of untreated (Fig. 3a) and treated cenospheres (Fig. 3b) in epoxy matrix. Higher magnification micrographs reveal poor interfacial bonding in untreated

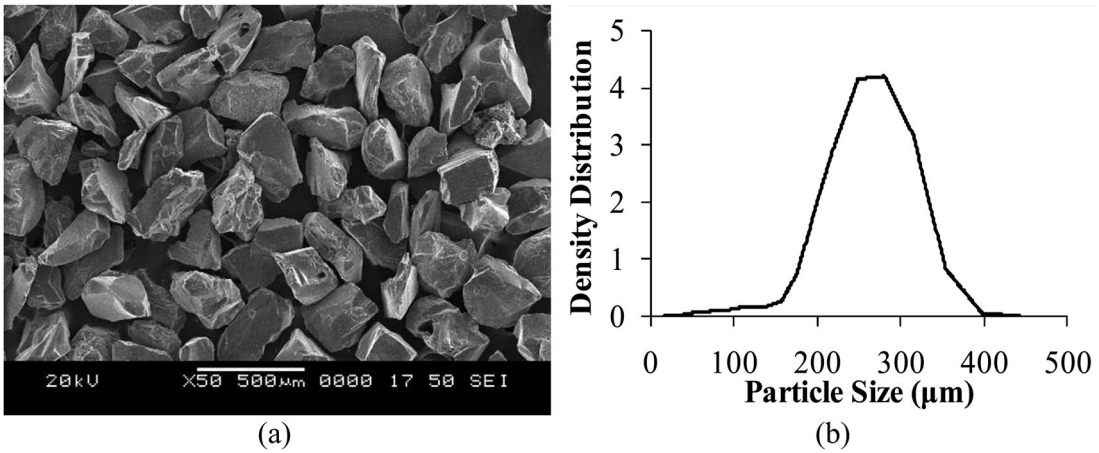

FIG. 2. (a) Micrograph of SiC erodent particles before test and (b) particle size analysis of erodent particles.

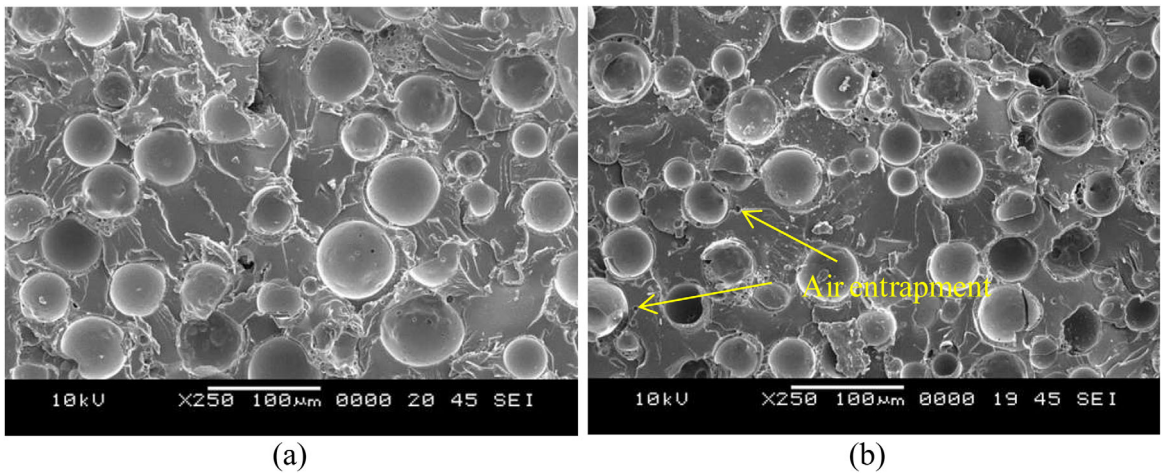

FIG. 3. Micrographs of as cast fractured (a) E60-U and (b) E60-T syntactic foams before test showing uniform dispersion of cenospheres.

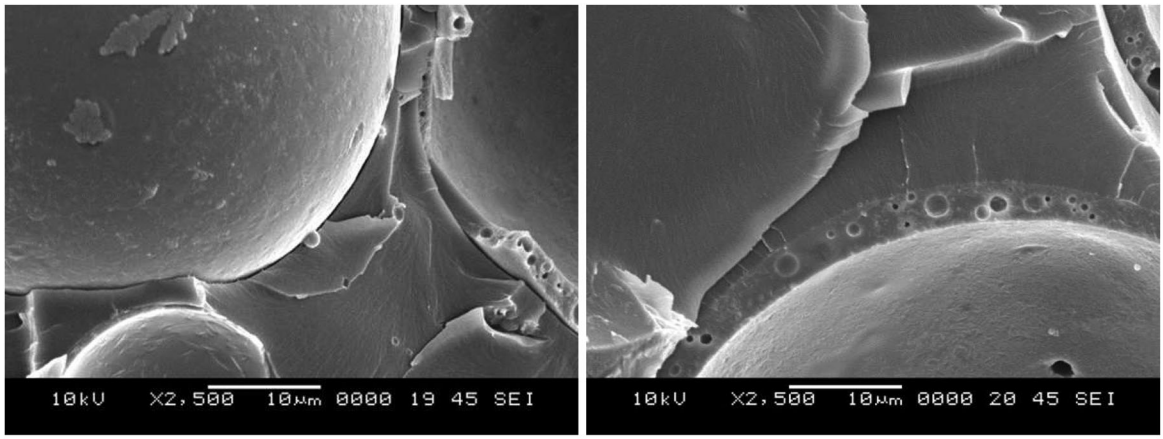

FIG. 4. (a) Lack of interfacial bonding is observed for E60-U whereas (b) seamless interfacial bonding is observed in E60-T.

cenospheres (Fig. 4a), while silane-treated cenospheres exhibit strong bonding (Fig. 4b) at the cenosphere-matrix interface. Shore hardness, density and matrix void content are presented in Table 2. Hardness of syntactic foams increases with increase in content of cenospheres for both untreated and surface treated cenospheres and is higher than that of the neat epoxy for all the syntactic foams. Improved interfacial bonding promoted by silane treatment of cenospheres has resulted in increased hardness of the specimens at comparable cenosphere content.

The matrix porosity content reduces the experimental density as compared with theoretical value. The matrix porosity content is limited to 3.7% in this case (Table 2), which is below the content reported by most studies for syntactic foams. Figure 3b indicates the matrix air porosity in a representative E60-T specimen. The size of the matrix pores appears to be an order of magnitude smaller than the cenospheres.

TABLE 2. Hardness, density and void volume fraction of samples [24]

Material	Shore Hardness	ρ^{th} (kg/m^3)	ρ^{exp} (kg/m^3)	φ_V (%)
E	64 ± 1.28	-	1192.00 ± 23.84	0.34
E20-U	68 ± 1.36	1137.60	1129.63 ± 22.59	0.70
E40-U	74 ± 1.48	1083.20	1064.72 ± 21.29	1.71
E60-U	78 ± 1.56	1028.80	1028.36 ± 20.56	0.05
E20-T	73 ± 1.46	1153.60	1133.14 ± 22.66	1.78
E40-T	77 ± 1.54	1115.20	1073.92 ± 21.47	3.70
E60-T	83 ± 1.66	1076.80	1055.65 ± 21.11	1.98

Steady State Erosion

Steady state of erosion needs to be attained to understand erosion type and mechanism. Table 3 presents the total mass of the erodent particles experimentally estimated to attain steady state erosion for all the materials at different velocities and impingement angles. For brevity, the standard deviations are not presented in the table but all the standard deviation values are within ±5% range. The erosion angle of the specimen surface is measured with respect to the direction of the particle impingement. The total particle mass required to attain steady state decreases with (1) increasing impingement angle, (2) decreasing velocity, (3) increasing filler content, and (4) silane coating. In all the cases, neat epoxy specimens require greater erodent particle mass to attain steady state compared with syntactic foams. Erodent mass required to attain the steady state is in the range of 75–175 g for all material types and the test conditions.

Figure 5 shows a representative set of erosion rate plots for all material types at lower (Fig. 5a) and higher impact angles (Fig. 5b) at intermediate velocity of 45 m/s. The first mass measurement is obtained after an initial testing period

TABLE 3. Erodent mass (g) for steady state erosion rate

	v = 30 m/s				v = 45 m/s				v = 60 m/s			
Material	30°	45°	60°	90°	30°	45°	60°	90°	30°	45°	60°	90°
E	115	105	105	95	145	125	115	115	175	155	155	145
E20-U	95	95	95	85	125	115	115	105	155	135	125	125
E40-U	95	85	85	75	115	115	105	95	135	115	115	115
E60-U	85	85	85	75	105	95	85	85	125	105	105	105
E20-T	95	95	95	95	115	105	105	95	135	125	125	115
E40-T	85	85	85	85	105	105	95	85	125	115	115	105
E60-T	85	85	75	75	95	95	85	75	115	105	105	95

DOI 10.1002/pc

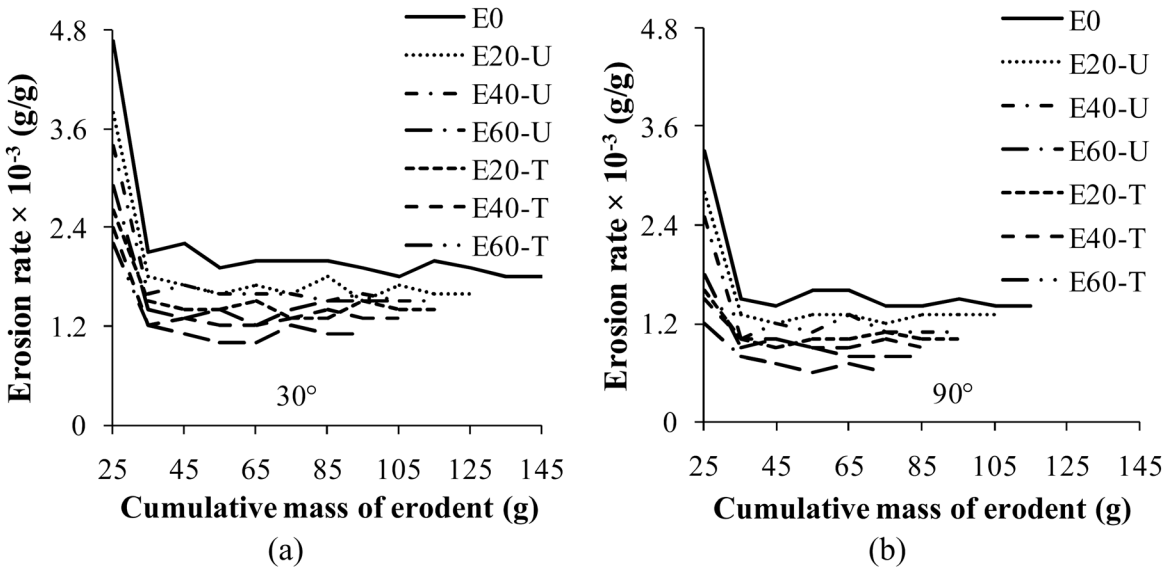

FIG. 5. Steady state erosion rate of all samples at v = 45 m/s for (a) 30° and (b) 90° impingement angles.

of 5 min, corresponding to 25 g of erodent. Cumulative erodent particle mass is observed to decrease drastically as the test progresses for the next 2 min. Repeated impact of erodent particles breaks the hard cenosphere particles in the matrix resulting in debris. The particle fracture is among the main energy absorption mechanisms; therefore, all

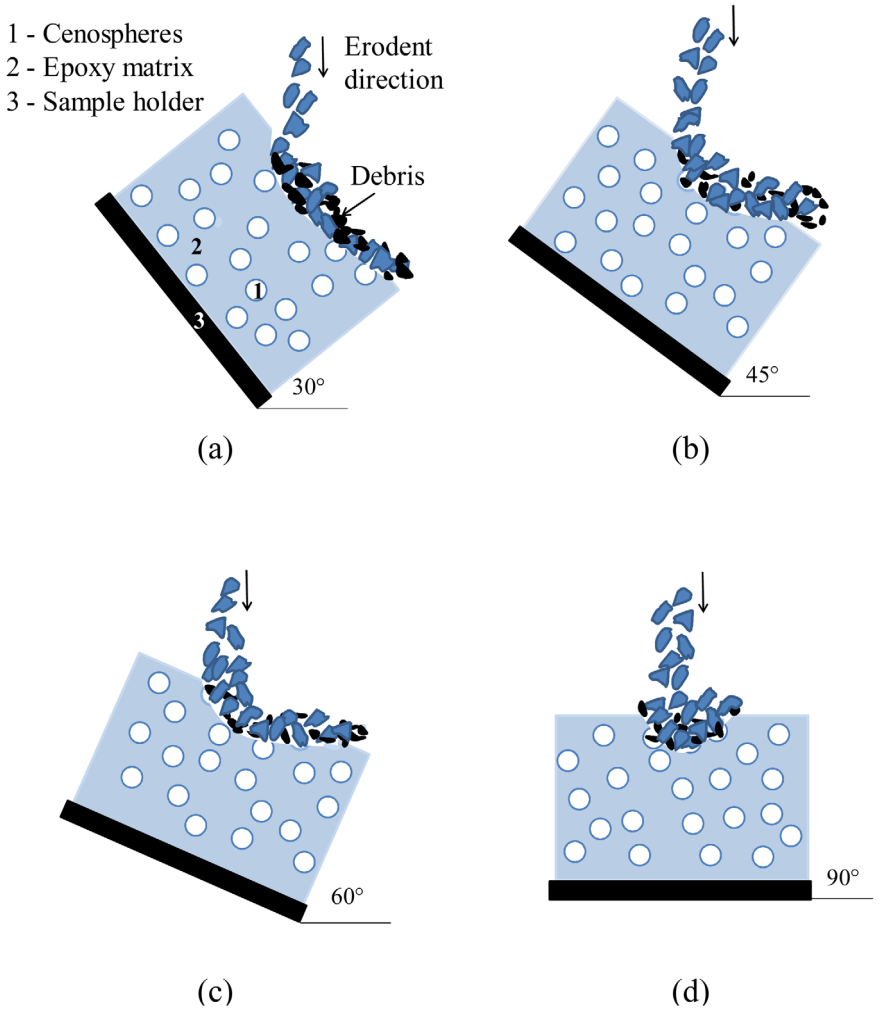

FIG. 6. Erosion mechanism in syntactic foams for (a) 30° (b) 45° (c) 60°, and (d) 90° impingement angles.

syntactic foams offer higher erosion resistance than the neat epoxy. With higher impact angles, erodent impingement is confined to smaller and more focused area resulting in attaining steady state much earlier (Fig. 5b) as compared with lower impact angles (Fig. 5a).

Figure 6 schematically represents of erosion mechanism in syntactic foams. Removal of erodent particles occurs easily over the surface at low angles 30° (Fig. 6a). Erodent particles impacting at lower angles impart sliding action on the specimen surface leading to easy removal of debris and

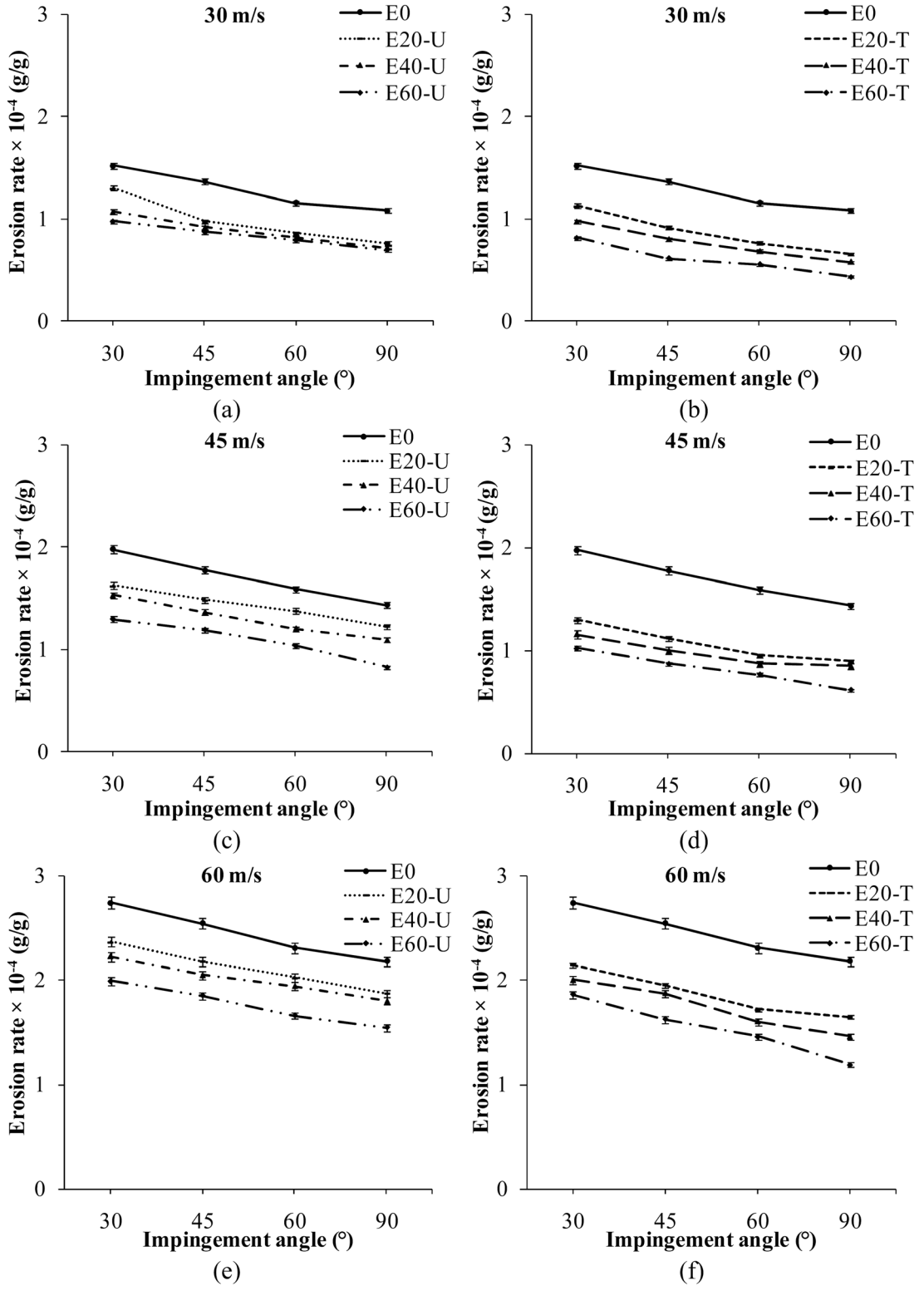

FIG. 7. Erosion rate of all samples at different velocities and impingement angles.

 DOI 10.1002/pc

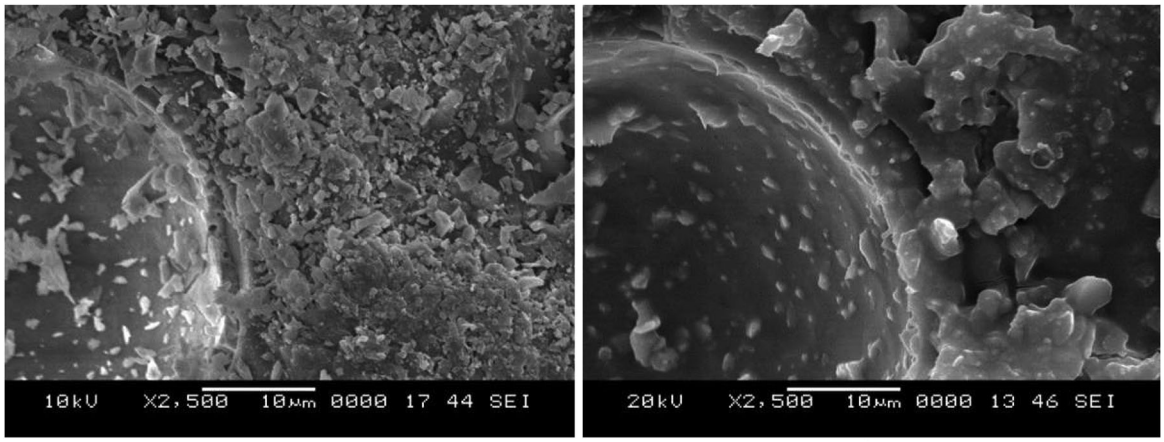

FIG. 8. Micrographs of representative syntactic foams for (a) E20-T and (b) E60-T.

higher erosion rate. Further, erodent particles are in contact with target surface for longer time resulting in higher material removal rate. Retention time of erodent on the sample surface decreases with increasing impingement angle (Fig. 6b–d) leading to lower erosion rates. Erosion rate decreases further at 90° owing to higher energy absorbing capabilities in foams under compression [26] as depicted by Fig. 6d. Neat epoxy specimens tend to exhibit higher erosion rates as compared with syntactic foams due to absence of cenospheres, which are made of ceramics and resist erosion better than the matrix resin.

Influence of Impingement Angle on Erosion

The erosion behavior strongly depends upon the experimental conditions and composition of target material [31]. Erosion rate of all the materials for different impingement angles are presented in Fig. 7. It is observed that the maximum erosion occurs at 30° for neat epoxy and decreases further with increasing impingement angle, similar to the observations in the previous studies [22,32–34]. The erosion rate recorded at 90° is at a relatively lower level as compared with that at 30° (Table 3). Impacting force resolves into normal and tangential components [35], which results in larger erosion area at low angles but deeper erosion pit at higher angles. With increase in angle of impact, the reduction in the tangential force reduces erosion rate. In all cases, syntactic foams have lower erosion rate than the neat resin because of the presence of ceramic cenospheres.

Influence of Filler Content on Erosion

Erosion resistance of syntactic foams containing untreated and silane-treated cenospheres is higher by 12–42 and 22–60%, respectively, compared with neat epoxy. Presence of ceramic particles increases the erosion resistance of syntactic foams compared with that of soft matrix resin. Silane treatment increases the particle–matrix interfacial strength in syntactic foams, which increases their

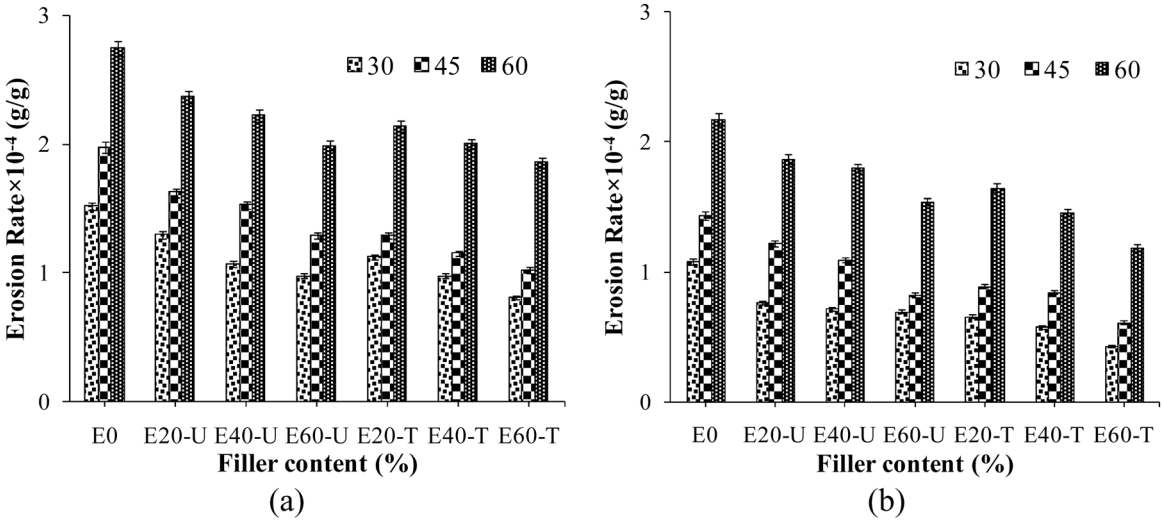

FIG. 9. Erosion rate as a function of erodent velocity at (a) 30° and (b) 90° impingement angles.

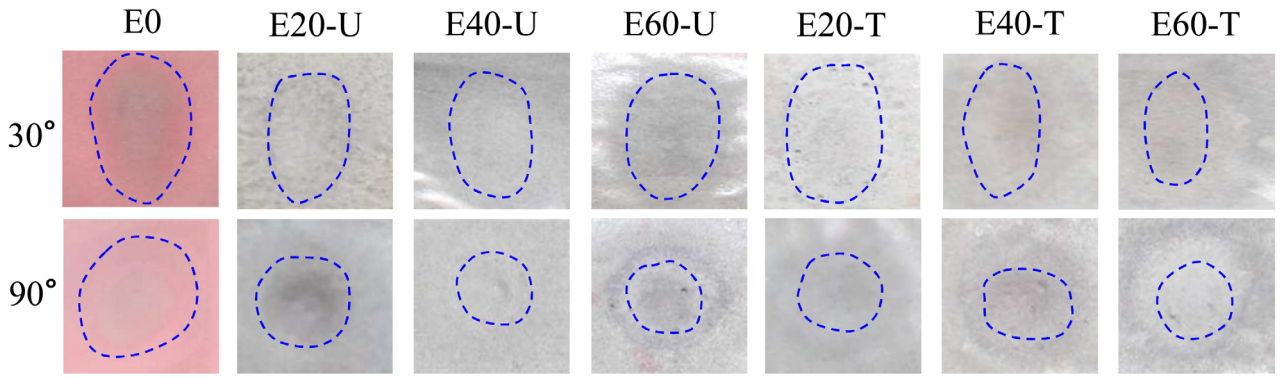

FIG. 10. Erosion scars in representative samples.

erosion resistance by 7–38% compared with syntactic foams containing untreated cenospheres. In the absence of strong interfacial bonding, cenospheres can be dislodged easily by the impinging erodent particles. In comparison, additional energy is required to break strongly bonded cenospheres and dislodge the debris from the matrix. Figure 8 presents micrographs of representative specimens after erosion test at lower (20 vol%) and higher (60 vol%) filler contents for foams containing surface treated cenospheres. Extensive erosion damage to the matrix is evident in the specimen containing higher volume fraction of matrix as seen in Fig. 8a.

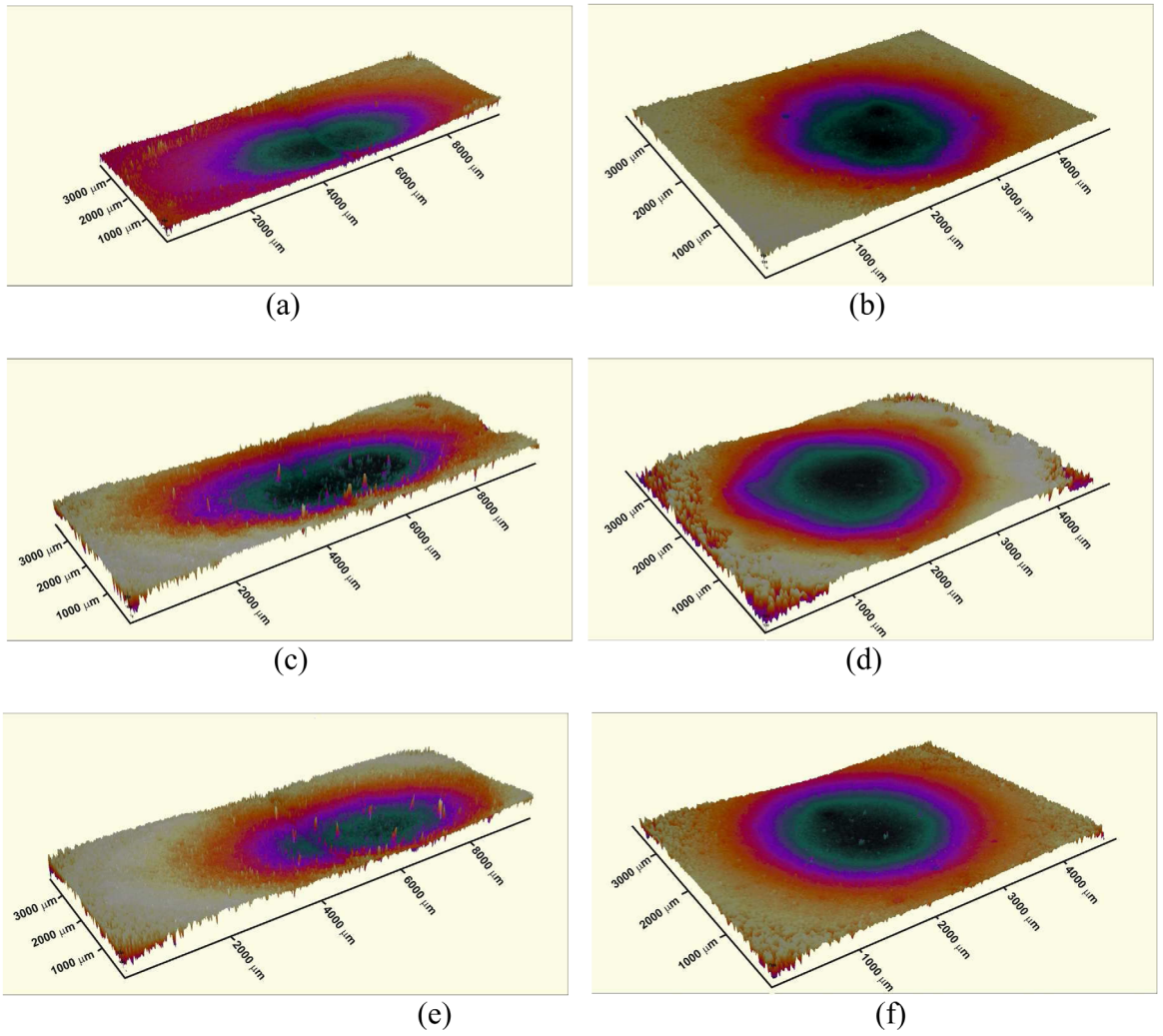

FIG. 11. Eroded profile of syntactic foams at 60 m/s for Neat epoxy (a) 30° and (b) 90°; E20-U at (c) 30° and (d) 90° and E20-T at (e) 30° and (f) 90°.

 DOI 10.1002/pc

Velocity Exponent and Erosion Efficiency

Velocity of the erodent particles influences material removal from the target surface as observed in Fig. 9a for lower and in Fig. 9b for higher impingement angles. Increase in erodent velocity increases the erodent flow per unit time impacting on the specimens, which in turn increases erosion. Erosion rate is observed to be up to 1.5 times higher as the velocity increases. Erosion rate (E_r) of polymer composites is characterized by velocity exponent "*n*", and is given by [36],

$$E_r \alpha v^n \tag{3}$$

where *v* is impact velocity expressed in m/s. *Eq. 3* is used to estimate *n* for all the materials using E_r and *v* values presented in Tables 1 and 3, respectively. Previous studies have established that materials are considered ductile or brittle based on the ranges $1 < n < 3$ or $3 < n < 5$, respectively [35]. In the present study, *n* values are in the range of 2.06–2.95, 2.03–2.81, and 2.0–2.68 for neat epoxy, EXX-U and EXX-T respectively, which indicates ductile behavior for all the materials presented herein. Erosion efficiency (ξ) is also a parameter used for identifying brittle and ductile erosion response of materials subjected to solid particle erosion. The erosion efficiency (ξ) is given by [37],

$$\xi = \frac{2E_r H}{\rho v^2} \tag{4}$$

Values of *v* (impact velocity), *H* (Shore Hardness), ρ (density), and E_r (steady state erosion rate) are used from Tables 1–3, respectively. Shore hardness values are converted to Pascal and used in *Eq. 4*. Ductile materials possess very low erosion efficiencies ($\xi < 10\%$) while for brittle materials its >100% [37,38]. For all the samples in the present case, ξ varies in the range of 0.046–0.177% for different impact velocities and impingement angles implying ductile erosive behavior. Higher erosion efficiency represents lower erosion resistance. Erosion efficiency of neat epoxy, EXX-U and EXX-T vary between 0.063–0.177, 0.060–0.171, and 0.046–0.138% respectively. From these observations it is clear that surface treated syntactic foams are suitable in erosive environment.

Surface Morphology of Eroded Surfaces

Figure 10 presents erosion surface profiles of a representative set of specimens of all material types. An elliptical shape of the damage zone is observed at 30°, whereas a circular shape is observed at 90°, which is consistent with the mechanism shown in Fig. 6. It is observed in Fig. 10 that the use of surface treated cenospheres in the highest volume fraction provides the smallest erosion profile on the material surface, indicating the benefit of cenosphere surface treatment under erosion conditions. Further observations of erosion profiles in 3D are presented in Fig. 11. It is observed that at 30° the eroded area is comparatively larger than that observed at normal angle of impact. At lower impact angles, the erodent particle removal from the surface is easier because of tangential velocity component of the material. In comparison, the normal impact results in erodent particles impinging on the existing erodent particles, which results in slow expansion of the erosion zone. Syntactic foams have lower erosion damage zone compared with the neat resin.

CONCLUSIONS

Solid particle erosion of cenosphere/epoxy syntactic foams is studied for variables such as impingement angle, impact velocity, and cenosphere content. Following conclusions are drawn:

- Lower impingement angles lead to higher erosion rate due to easy removal of material from the surface and continuous exposure of fresh surface of the specimen. The observations of erosion rate are supported by surface and volume profiles of the erosion area, where lower angles show larger damage zone.
- When compared with neat epoxy, erosion resistance of syntactic foams is higher due to the presence of ceramic reinforcement. Surface treatment of cenospheres improves particle-matrix interfacial bonding and reduces erosion rate.
- Silane treatment of cenospheres has increased the erosion resistance of EXX-T foams and is in the range of 7–38% as compared with EXX-U foams. E60-T foams exhibit highest erosion resistance among all the samples.

ACKNOWLEDGMENT

Mrityunjay Doddamani acknowledges Department of Science and Technology, India, Grant DST/TSG/AMT/2015/394/G. Nikhil Gupta acknowledges Office of Naval Research Grant N00014-10-1-0988. The views expressed in this article are those of the authors, not of funding agencies. The authors would like to thank the ME Department at NIT-K and NYU for providing facilities and support.

REFERENCES

1. N. Gupta, S.E. Zeltmann, V.C. Shunmugasamy, and D. Pinisetty, *JOM*, **66**(2) 245 (2014).
2. S.E. Zeltmann, K.A. Prakash, M. Doddamani, and N. Gupta, *Composites Part B: Engineering*, **120** 27 (2017).
3. M.L. Jayavardhan, B.R. Bharath Kumar, M. Doddamani, A. K. Singh, S.E. Zeltmann, and N. Gupta, *Composites Part B: Engineering*, **130** 119 (2017).
4. R.N. Rothon. in Mineral Fillers in Thermoplastics: Filler Manufacture and Characterisation, in Mineral Fillers in Thermoplastics I: Raw Materials and Processing, Vol. **67–107**, J. Jancar, E. Fekete, P.R. Hornsby, J. Jancar, B. Pukánszky, and R.N. Rothon, Eds. Berlin, Heidelberg, Springer Berlin Heidelberg (1999).

5. A.K. Singh, B. Patil, N. Hoffmann, B. Saltonstall, M. Doddamani, and N. Gupta, *JOM*, **70**(3) 303 (2018).
6. A.K. Singh, B. Saltonstall, B. Patil, N. Hoffmann, M. Doddamani, and N. Gupta, *JOM*, **70**(3) 310 (2018).
7. J.L. Acosta, E. Morales, M.C. Ojeda, and A. Linares, *Die Angewandte Makromolekulare Chemie*, **138**(1) 103 (1986).
8. M. Labella, S.E. Zeltmann, V.C. Shunmugasamy, N. Gupta, and P.K. Rohatgi, *Fuel*, **121**(Supplement C) 240 (2014).
9. V. Manakari, G. Parande, M. Doddamani, V.N. Gaitonde, I. G. Siddhalingeshwar, Kishore, V.C. Shunmugasamy, and N. Gupta, *Tribology International*, **92**(Supplement C) 425 (2015).
10. M.M. Hossain and K. Shivakumar, *Composite Structures*, **94**(1) 290 (2011).
11. M. Doddamani, Kishore, V.C. Shunmugasamy, N. Gupta, and H.B. Vijayakumar, *Polymer Composites*, **36**(4) 685 (2015).
12. B. Wetzel, F. Haupert, K. Friedrich, M.Q. Zhang, and M. Z. Rong, *Polymer Engineering & Science*, **42**(9) 1919 (2002).
13. R.V. Kurahatti, A.O. Surendranathan, S. Srivastava, N. Singh, A.V. Ramesh Kumar, and B. Suresha, *Materials & Design*, **32**(5) 2644 (2011).
14. K. Rugele, D. Lehmhus, I. Hussainova, J. Peculevica, M. Lisnanskis, and A. Shishkin, *Materials*, **10**(7) 828 (2017).
15. A. Shishkin, V. Mironov, V. Zemchenkov, M. Antonov, and I. Hussainova, *Key Engineering Materials*, **674** 35 (2016).
16. J. Baronins, J. Setina, G. Sahmenko, S. Lagzdina, and A. Shishkin, *IOP Conference Series: Materials Science and Engineering*, **96**(1) 012011 (2015).
17. A.P. Harsha, U.S. Tewari, and B. Venkatraman, *Wear*, **254**(7) 693 (2003).
18. A.P. Harsha and A.A. Thakre, *Wear*, **262**(7) 807 (2007).
19. N.M. Barkoula and J. Karger-Kocsis, *Wear*, **252**(1) 80 (2002).
20. A. Hager, F., K, Y.A. Dzenis, and S.A. Paipetis. "*Study of erosion wear of advanced polymer composites*," in Proceeding of ICCM 10. Cambridge, UK, Woodhead Publishing (1995).
21. G.P. Tilly and W. Sage, *Wear*, **16**(6) 447 (1970).
22. A. Patnaik, A. Satapathy, N. Chand, N.M. Barkoula, and S. Biswas, *Wear*, **268**(1) 249 (2010).
23. J. Abenojar, J. Tutor, Y. Ballesteros, J.C. del Real, and M. A. Martínez, *Composites Part B: Engineering*, **120** 42 (2017).
24. N. Gamze Karsli, T. Yilmaz, A. Aytac, and G. Ozkoc, *Composites Part B: Engineering*, **44**(1) 385 (2013).
25. B.R. Bharath Kumar, M. Doddamani, S.E. Zeltmann, N. Gupta, S.G. Uzma, and R.R.N. Sailaja, *Journal of Materials Science*, **51**(8) 3793 (2016).
26. K. Shahapurkar, C.D. Garcia, M. Doddamani, G.C. Mohan Kumar, and P. Prabhakar, *Composites Part B: Engineering*, **135**(Supplement C) 253 (2018).
27. ASTM G76-13, *Standard Test Method for Conducting Erosion Tests by Solid Particle Impingement Using Gas Jets*, ASTM International, PA, USA.
28. V.K. Srivastava and A.G. Pawar, *Composites Science and Technology*, **66**(15) 3021 (2006).
29. A. Satapathy, A. Patnaik, and M.K. Pradhan, *Materials & Design*, **30**(7) 2359 (2009).
30. A.P. Harsha and S.K. Jha, *Wear*, **265**(7) 1129 (2008).
31. I.M. Hutchings, *Journal of Physics D: Applied Physics*, **25**(1A) A212 (1992).
32. N. Miyazaki and N. Takeda, *Journal of Composite Materials*, **27**(1) 21 (1993).
33. M. Bagci and H. Imrek, *Tribology International*, **44**(12) 1704 (2011).
34. M. Bagci and H. Imrek, *Materials & Design*, **46** 706 (2013).
35. K.C. Goretta, N. Chen, F. Gutierrez-Mora, J.L. Routbort, G. C. Lukey, and J.S.J. van Deventer, *Wear*, **256**(7) 714 (2004).
36. K.V. Pool, C.K.H. Dharan, and I. Finnie, *Wear*, **107**(1) 1 (1986).
37. G. Sundararajan, M. Roy, and B. Venkataraman, *Wear*, **140**(2) 369 (1990).
38. M. Mathapati, M.R. Ramesh, and M. Doddamani, *Surface and Coatings Technology*, **325**(Supplement C) 98 (2017).